ARL-TR-9507 ● AUG 2022

DEVCOM ARMY RESEARCH LABORATORY

Design, Inspection, and Testing of As-Built and Infiltrated Additively Manufactured Aluminum Lattice Truss Structures

by Marc Pepi, Jennifer Sietins, Rich Martukanitz, Corey Dickman, Ken Meinert, Rik Riman, Paul Moy, Vincent Wu, Ray Wildman, Mingling Tao, and Mengxuan Zhao

NOTICES

Disclaimers

The findings in this report are not to be construed as an official Department of the Army position unless so designated by other authorized documents.

Citation of manufacturer's or trade names does not constitute an official endorsement or approval of the use thereof.

Destroy this report when it is no longer needed. Do not return it to the originator.

ARL-TR-9507 ● AUG 2022

Design, Inspection, and Testing of As-Built and Infiltrated Additively Manufactured Aluminum Lattice Truss Structures

Marc Pepi, Jennifer Sietins, Paul Moy, Vincent Wu, and Ray Wildman
DEVCOM Army Research Laboratory

Rich Martukanitz, Corey Dickman, and Ken Meinert
Penn State University Applied Research Laboratory

Rik Riman
Rutgers University

Mingling Tao and Mengxuan Zhao
Worcester Polytechnic Institute

REPORT DOCUMENTATION PAGE

Form Approved
OMB No. 0704-0188

1. REPORT DATE *(DD-MM-YYYY)*	2. REPORT TYPE	3. DATES COVERED (From - To)
August 2022	Technical Report	1 October 2016–30 September 2018

4. TITLE AND SUBTITLE
Design, Inspection, and Testing of As-Built and Infiltrated Additively Manufactured Aluminum Lattice Truss Structures

5a. CONTRACT NUMBER

5b. GRANT NUMBER

5c. PROGRAM ELEMENT NUMBER

6. AUTHOR(S)
Marc Pepi, Jennifer Sietins, Rich Martukanitz, Corey Dickman, Ken Meinert, Rik Riman, Paul Moy, Vincent Wu, Ray Wildman, Mingling Tao, and Mengxuan Zhao

5d. PROJECT NUMBER

5e. TASK NUMBER

5f. WORK UNIT NUMBER

7. PERFORMING ORGANIZATION NAME(S) AND ADDRESS(ES)
DEVCOM Army Research Laboratory
ATTN: FCDD-RLW-MD
Aberdeen Proving Ground, MD 21005

8. PERFORMING ORGANIZATION REPORT NUMBER
ARL-TR-9507

9. SPONSORING/MONITORING AGENCY NAME(S) AND ADDRESS(ES)

10. SPONSOR/MONITOR'S ACRONYM(S)

11. SPONSOR/MONITOR'S REPORT NUMBER(S)

12. DISTRIBUTION/AVAILABILITY STATEMENT
Approved for public release: distribution unlimited.

13. SUPPLEMENTARY NOTES
ORCID ID: Marc Pepi, 0000-0003-0691-5925

14. ABSTRACT
Lightweight aluminum-alloy lattice truss structures were designed for optimized compressive strength and additively manufactured using the direct metal laser-sintering technique. A number of the trusses were infiltrated with a low-temperature solidified ceramic and a geopolymer formulation, both environmentally favorable alternatives to Portland cement. Some trusses were infiltrated with dicyclopentadiene for comparison. Micro-computed tomography inspection was performed prior to compression testing and detected microcracks in both the fill materials and actual trusses as well as porosity within the fill materials. This information was useful in predicting the comparative compressive strength of the infiltrated trusses.

15. SUBJECT TERMS
Science of Extreme Materials, additive manufacturing, topology optimization, mechanical properties, aluminum alloy AlSi10Mg, laser powder bed fusion, lattice structures

16. SECURITY CLASSIFICATION OF:			17. LIMITATION OF ABSTRACT	18. NUMBER OF PAGES	19a. NAME OF RESPONSIBLE PERSON
a. REPORT	b. ABSTRACT	c. THIS PAGE			Marc Pepi
Unclassified	Unclassified	Unclassified	UU	37	19b. TELEPHONE NUMBER (Include area code) (410) 306-0848

Standard Form 298 (Rev. 8/98)
Prescribed by ANSI Std. Z39.18

Contents

List of Figures

List of Tables

Acknowledgments

The authors wish to thank Mick Maher, DARPA Program Manager for “Open Manufacturing” for funding that allowed Penn State University to additively manufacture the aluminum trusses.

1. Introduction

Metal additive manufacturing (AM) may someday exist on the battlefield, and indigenous or other materials may be on hand for enhanced performance of these AM builds. With respect to how advanced manufacturing at the point of need can benefit the military, General Gus Perna (former commanding general of the U.S. Army Materiel Command (AMC) said, "advanced manufacturing enhances the supply chain and sustainment efforts, forward in the field enabling soldiers to quickly manufacture critical parts and supplies".[1] Toward this vision, metallic trusses were additively manufactured and subsequently infiltrated with various materials, forming hybrid structures to show the "art of the possible" for potentially unique on-demand ballistic and or blast protection. Compression testing and impact resistance have been shown to be correlated,[2] which was why compression testing was chosen for this study. Cellular materials such as trusses offer an advantageous combination of high strength and low weight. Lattice structures composed of a monolithic material and space can be divided into two categories[3]: stochastic (foam) structures and periodic structures (truss-like). Metallic foams were considered for this research; however, there were two negatives associated with this choice. First, it was believed that AM metallic trusses would be easier than metallic foams to manufacture in-theater. Second, it has been shown that lattice structures are about three times stronger than metallic foam of the same material since the foam is governed by cell wall bending while the lattice elements stretch and compress.[4]

As a proof-of-concept, the US Army Combat Capabilities Development Command Army Research Laboratory collaborated with Penn State University/Applied Research Laboratory/Center for Innovative Materials Processing through Direct Digital Deposition (CIMP-3D) to produce 40- × 40- × 40-mm aluminum alloy trusses fabricated using the EOS M280 powder bed fusion process. The design was optimized for compression loading using topology optimization at DEVCOM Army Research Laboratory. Some of the trusses were infiltrated with a low-temperature solidified (LTS) ceramic, others with a geopolymer, and the remainder with dicyclopentadiene (DCPD). Their properties were compared to those of as-built trusses. Each of the trusses were inspected by micro-computed tomography (micro-CT) prior to compression testing.

2. Materials and Methods

2.1 Design

The structure shown in Fig. 1 was designed using topology optimization, an automated design technique that produces an optimal structure subject to a given set of loads and boundary conditions.[5] In particular, a standard isotropic linear elastic topology optimization technique (as outlined in Liu and Tovar[5]) was used to optimize a unit-cell (discretized at a step size of 0.4 mm along each direction) for compression with a volume fraction constraint of 25%. Rather than pure compression, however, four additional shear loads (in the $\pm x$-directions and $\pm y$-directions) of half the magnitude of the compressive load were also included. The shear loads were applied on the top surface and were included to generate a more robust structure. While the structure was intended to be filled, no filling material was assumed—only void. Further, no steps were taken to ensure (or improve) the manufacturability of the structure. To generate the final structure, the unit cell was then repeated five times along each dimension and the resulting topology was postprocessed using the Computational Geometry Algorithms Library (CGAL).[6]

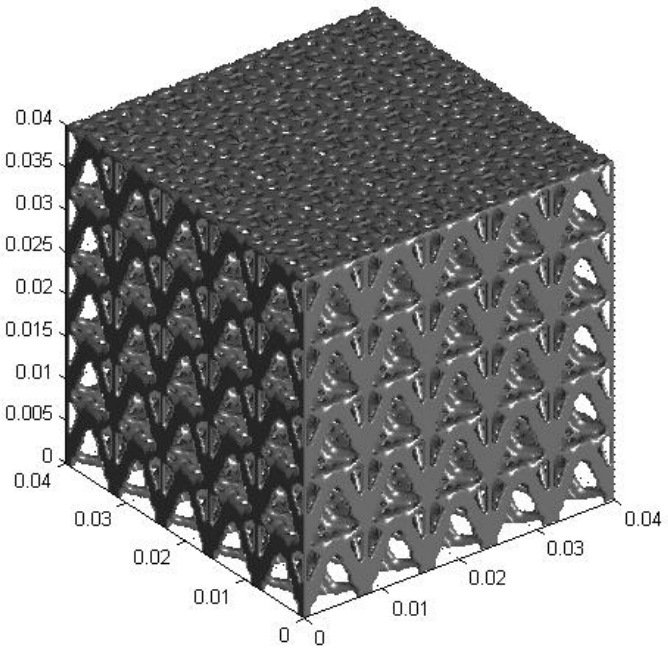

Fig. 1 Design of metallic truss optimized for compressive loading via topology optimization

2.2 Specimen Manufacturing

Sixteen aluminum trusses were manufactured with an EOS M280 via the direct metal laser-sintering (DMLS) process. This process is the most popular for the AM of metallic powders,[7] and uses an ytterbium fiber laser in an argon atmosphere to melt the metal powder with a continuous power up to 370 W and a spot size of 70–80 μm. The DMLS process builds parts layer by layer from a metal powder bed based on a sliced representation of an .stl file. The aluminum powder used for this build was EOS AlSi10Mg (EOS part no 9011-0024), patterned after aluminum 356/360 type casting alloys having good castability properties. The parts were fabricated on an aluminum build plate, then subjected to a post-heat-treatment process. On average, the 40-mm cubed trusses weight approximately 47 g each. Representative trusses are shown in Fig. 2 (side and top view).

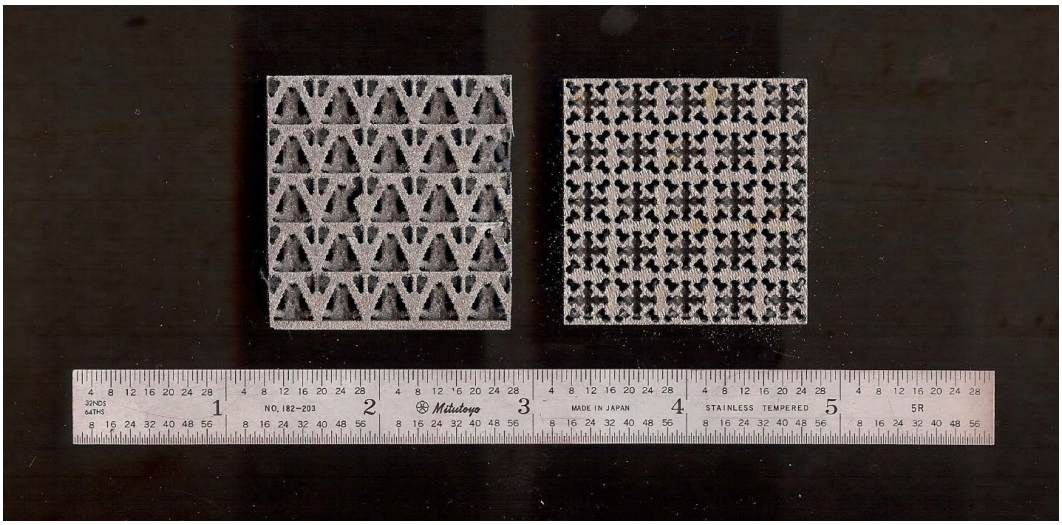

Fig. 2 Representative as-built aluminum trusses after AM build: (left) side view, (right) top view

2.3 Specimen Heat Treatment

As built, the aluminum trusses exhibit considerable free silicon and significant grain boundary precipitation, as well as low strength and fairly low ductility.[8] The trusses that were still on the build plate were subjected to a solution heat treatment of approximately 575 °C for 15 min followed by water quench, and the aging process was performed at 226 °C for 8 h. A significant improvement in strength and some improvement in ductility were expected from the solution heat treatment and aging, A stress relief during the solution heat treatment process was also accomplished (2 h at 250 °C) to reduce significant residual stresses of the as-built material. After this process, the trusses were removed from the build plate via electro-discharge machining (EDM).

2.4 Infiltration with Low-Temperature Solidified Ceramic

Three of the aluminum trusses were infiltrated with LTS ceramic. The weights of the three LTS-infiltrated trusses plus the LTS are shown in Table 1. These weights were roughly three times that of the original trusses.

Table 1 Weight of LTS-infiltrated trusses

Sample	Weight (g)
1	159.4
2	158.2
3	155.8

This material has been shown to be an effective alternative to Portland cement with many advantages, including little to no shrinkage, no use of toxic materials, carbon consumer versus carbon producer, and more. LTS solidifies through reactive hydrothermal (solvothermal) liquid phase densification (rHLPD). This solvothermal technology enables ceramic densification to proceed without high-temperature kilns. Rutgers University invented rHLPD and has used it to densify a wide range of monolithic composite systems that include ceramics, metals, and polymers.[9] Their discovery of the calcium silicate (calcium carbonate–silicon dioxide) ($CaSiO_3$ [$CaCO_3$,-SiO_2]) composite system as a suitable cementitious phase for concrete is beginning to displace Portland cement in the commercial market. Cement and concrete companies are licensing this technology because the materials have exceptional properties (e.g., strength and durability), meet industry 2050 CO_2 emissions and energy goals, and match the cost of ordinary Portland cement.

The LTS process presents an opportunity to use metallic trusses as scaffolding for metal–ceramic structural composites. Since the LTS of ceramics does not require the high temperature of conventional ceramic hardening techniques, metal structures can be incorporated without fear of deformation or melting, which is particularly important for aluminum. Its low density (2.7 g/cm^3) is attractive for low-weight structures, but its melting point (660 °C) prevents it from maintaining any structure during ceramic sintering (usually >1,000 °C). Typical LTS processes rarely exceed 200 °C, and for the infiltration of aluminum trusses described herein, only 90 °C was used in processing. Thus, aluminum structures can be infiltrated with a ceramic suspension, and the ceramic can subsequently be hardened in place without damaging the aluminum.

To investigate metal–ceramic composites formed via infiltration of LTS, aluminum trusses were infiltrated with $CaSiO_3$ and solidified. The intent of this research was to create a system that might provide improved mechanical properties over

traditional concrete, or aluminum trusses on their own. LTS was infiltrated into 40-mm cubes for compression testing. Figure 3 shows an LTS-infiltrated aluminum truss.

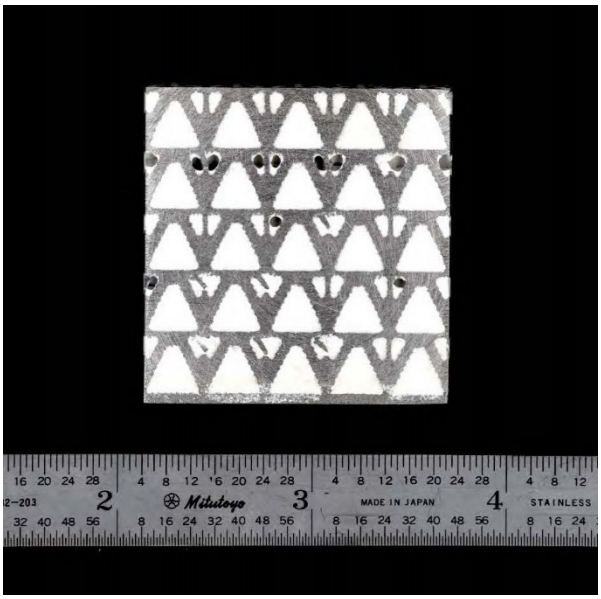

Fig. 3 LTS-infiltrated aluminum truss

2.5 Infiltration with Geopolymer

Four trusses were infiltrated with a geopolymer formulation containing red mud slurry and Class F fly ash. This material is formed by the reaction of amorphous silica and alumina-rich solids with a high alkaline solution and can also be used as an alternative to conventional construction materials. Recently, this material has been the subject of significant research due to its exceptional mechanical, chemical, and physical properties and the potentially broad practical applications in civil infrastructure construction, waste encapsulation, and sustainable development.[10] As Table 2 shows, the recipe also included $CaSiO_3$ solution, sodium hydroxide (NaOH), Si/aluminum (Al), sodium (Na)/Al, and water. Red mud slurry is a byproduct of the alumina refining process, and Class F fly ash is produced by the burning of anthracite and bituminous coal. Figure 4 shows a geopolymer-infiltrated aluminum truss. The properties of this recipe as reported by Worcester Polytechnic Institute are listed in Table 3. The geopolymer was cured at 50 °C for 7 days followed by room temperature curing for 21 days. The final weights of the infiltrated trusses are shown in Table 4. Note that these trusses weigh a little more than half the weight of the LTS-infiltrated trusses.

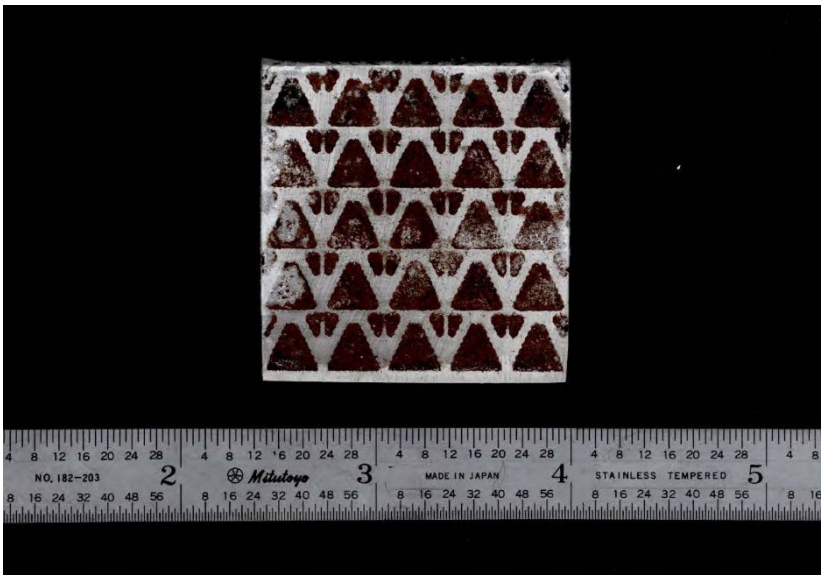

Fig. 4 Geopolymer-infiltrated aluminum truss

Table 2 Geopolymer recipe

Red mud slurry (g)	Class F fly ash (g)	$CaSiO_3$ solution (mL)	50% NaOH (mL)	Si/Al (mol)	Na/Al (mol)
120	480	74	52	2.00	0.60

Table 3 Geopolymer properties

Liquid/solid (weight ratio)	Water content (wt%)	UCS[a] (MPa)
0.53	25	18.9

[a] UCS = unconfined compressive strength

Table 4 Weight of geopolymer-infiltrated trusses

Sample	Weight (g)
1	94.9
2	88.4
3	93.1
4	96.8

2.6 Infiltration with Dicyclopentadiene

Dicyclopentadiene resin, or DCPD, is a chemical compound also known as $C_{10}H_{12}$. This resin has been shown to be a tough, rigid, thermoset polymer with high modulus, and excellent impact strength and chemical resistance. As a result of this combination of properties, the material finds extensive use in a variety of applications that require toughness and chemical resistance.[11,12] Although it may be impractical to believe that this material would be available at the point of need, it was included here for comparison to the results of the other infiltration materials. Trusses were infiltrated by SullyPower LLC using a DCPD monomer, ESM 610, from Spencer Composites Corporation of California. Ruthenium catalyst by Umicore M1 was chosen for the base catalyst. The ratio of ESM 610 to Umicore M1 was 12,000 to 1. The resin was infiltrated into the lattices in a proprietary fashion that was not divulged. However, since the DCPD and the catalyst used in the resin are sensitive to water and oxygen, it is surmised that curing was performed in a vacuum. This polymer does not need elevated temperature curing; however, without it the product will not attain full properties, and there will be residual unreacted monomer in the sample that will be evident by an outgassing odor. Since the samples under investigation did exhibit an odor, it is surmised that an elevated temperature cure was not performed.[13] Images of the DCPD-infiltrated trusses are shown in Fig. 5. The weights of the DCPD-infiltrated trusses are shown in Table 5 and were comparable to those of the geopolymer-infiltrated trusses.

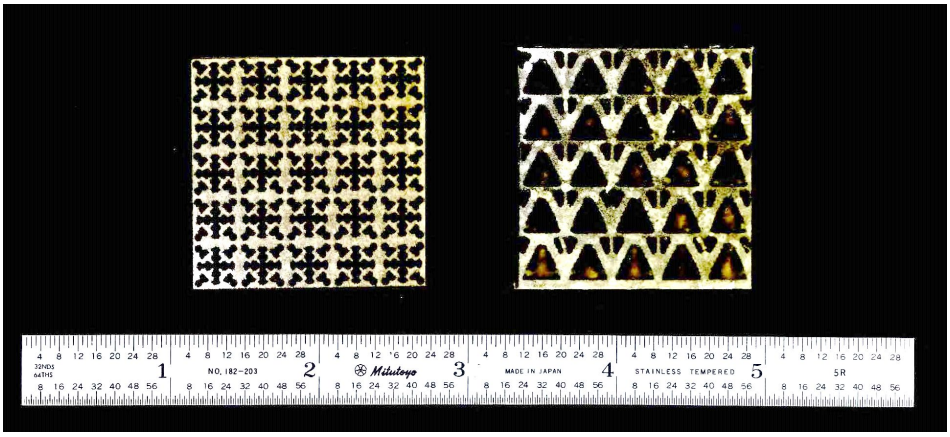

Fig. 5 DCPD-infiltrated aluminum trusses

Table 5 Weight of DCPD-infiltrated trusses

Sample	Weight (g)
1	98.4
2	97.9
3	97.6
4	97.4

3. Inspection Results

3.1 Micro-CT – LTS-Infiltrated Trusses

The as-built metallic trusses and those infiltrated with LTS were subjected to X-ray micro-CT inspection prior to compression testing. A Zeiss Xradia 520 Versa was used to scan an aluminum truss without any infiltration (Fig. 6, left) as well as after the LTS infiltration (Fig. 6, right). A scanning voltage of 80 kV was used for the unfilled truss and 160 kV for the infiltrated truss in order for the X-rays to have enough power for transmission through the entire sample. The voxel sizes were 56.6 and 56.2 μm, respectively. As seen in the infiltrated truss, large voids were present where the ceramic did not fully impregnate the truss structure. Figure 7 shows microcracks within the LTS, perhaps forming during solidification.

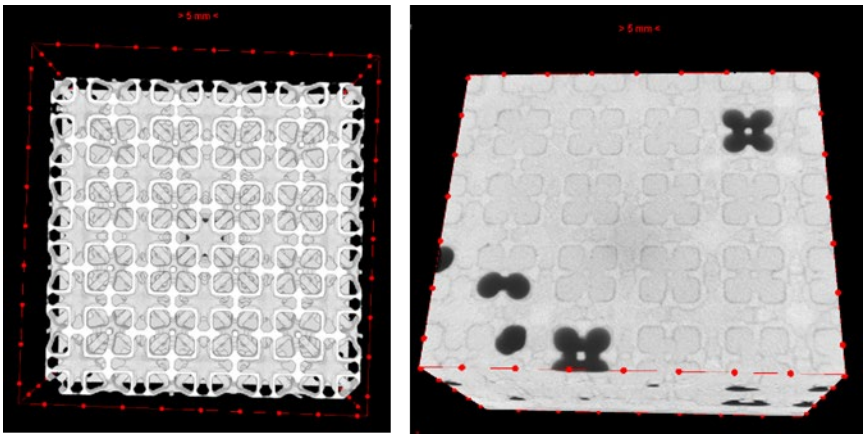

Fig. 6 X-ray CT scan of the aluminum truss (left) and LTS-infiltrated truss (right). There is a 5-mm spacing between the red dots.

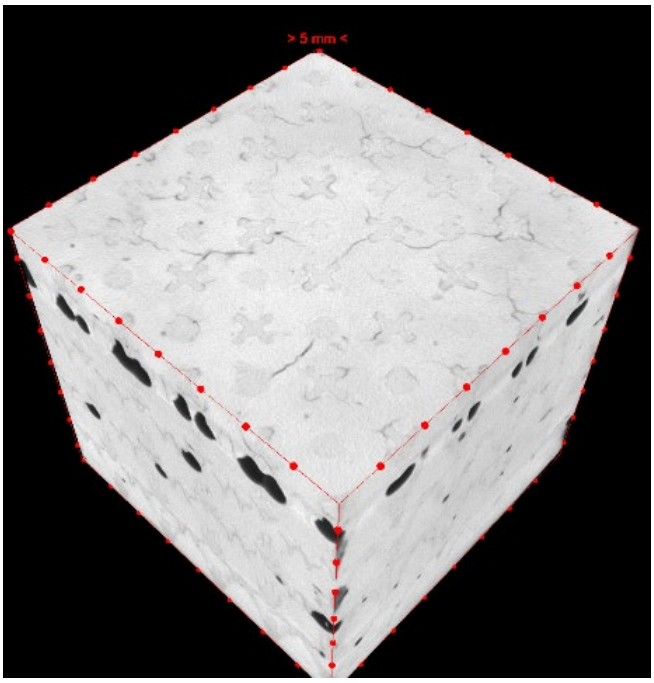

Fig. 7 Microcracks within the LTS of an inspected truss

Additionally, higher-resolution scans were conducted on approximately one unit cell of both structures. The same scanning voltages of 80 and 160 kV were used with resolutions of 14.8 and 14.3 μm/voxel for the non-filled and filled trusses. The higher resolution provided additional information that was not evident in the previous scans. Micro-porosity within the truss ligaments were observed in the non-filled truss (Fig. 8, left). The red arrows indicate a few selected locations with micro-porosity. Additionally, rough surfaces were observed with the higher-resolution scan. This may make the infiltration process more challenging by restricting flow, especially near the aluminum–ceramic interfaces. This is further supported by the higher-resolution scan of the filled truss (Fig. 8, right) where small gaps can be seen between the truss and filling material.

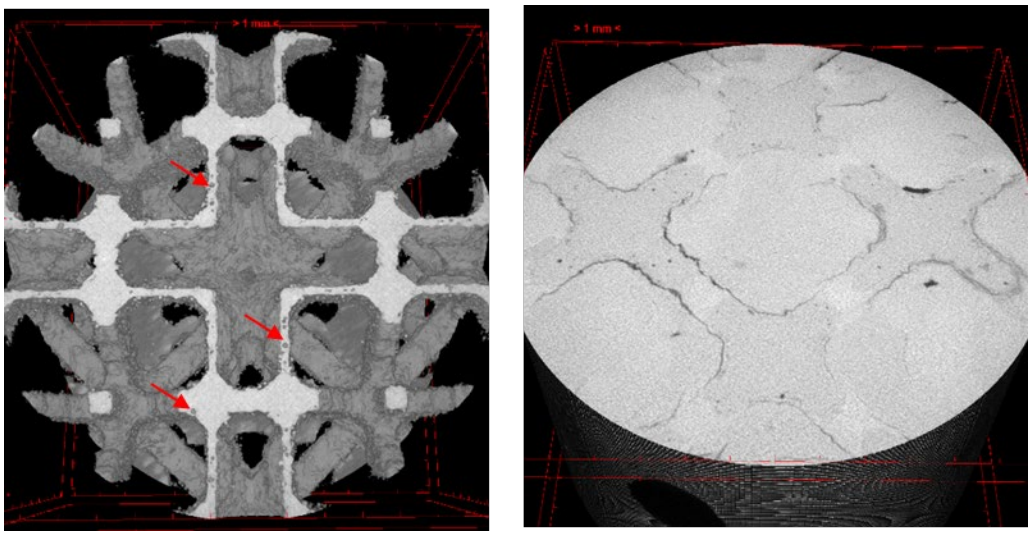

Fig. 8 Higher-resolution CT scans of the aluminum truss showing micro-porosity within the truss ligaments (left) and gaps at the aluminum/ceramic interfaces (right). Scale bar represents 1 mm.

Analysis was performed on the LTS-filled trusses to quantify the degree of infiltration. Bruker Skyscan CTAn software was used to segment the air within the sample volume, and porosity percentages were calculated as a function of the sample height. The results are shown in Fig. 9 and show that there were problematic layers corresponding with the truss unit cell geometry where there was difficulty filling. The average percent porosities through the entire sample volumes were 2.6%, 4.4%, and 5.4% for samples 1–3, respectively. It is important to note, however, that sample 2 had the maximum peak porosity within any given 2-D layer through the sample height at 35.2%. Sample 3 had a peak porosity of 34.0%, and sample 1 had the lowest peak porosity of the three samples at 27.5%.

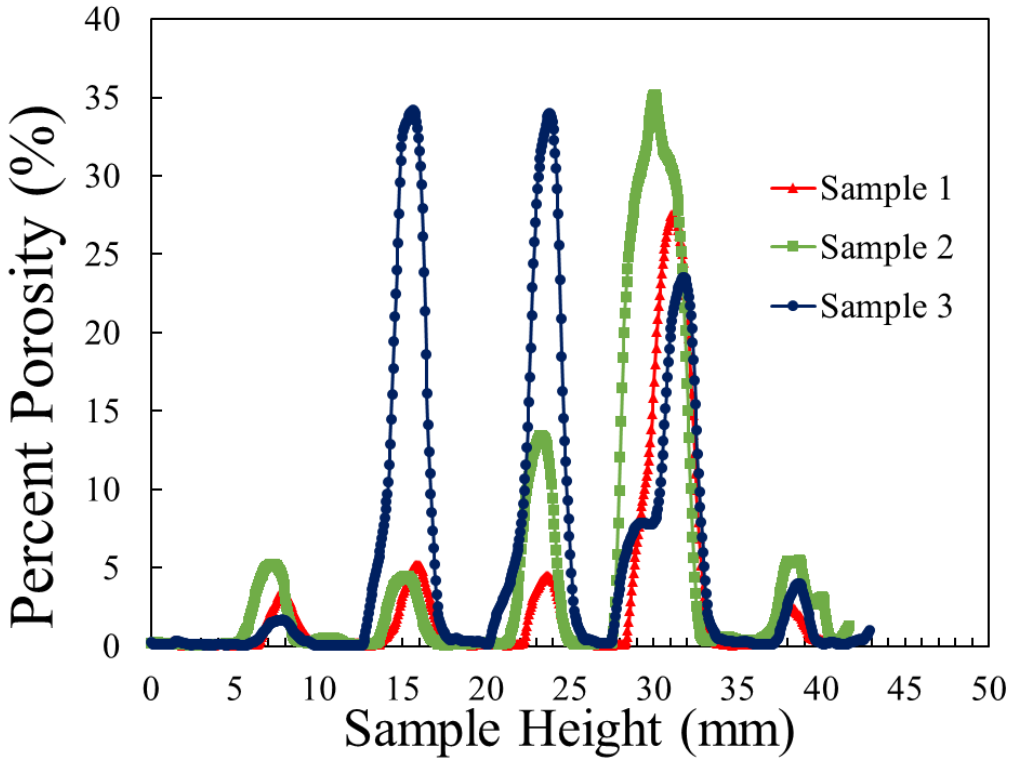

Fig. 9 Percent porosity of the LTS infiltrated trusses as a function of sample height

3.2 Micro-CT – Geopolymer-Infiltrated Trusses

A similar micro-CT analysis was performed on the geopolymer-filled trusses, and the results are shown in Fig. 10. There were large variations in porosity percentages for every sample. The maximum porosity was 64.2% (sample 2), and the minimum was 2.3% (sample 1), as shown in the image slices in Fig. 10. The average porosity ranged from 26.8% for sample 4 to 38.0% for sample 2.

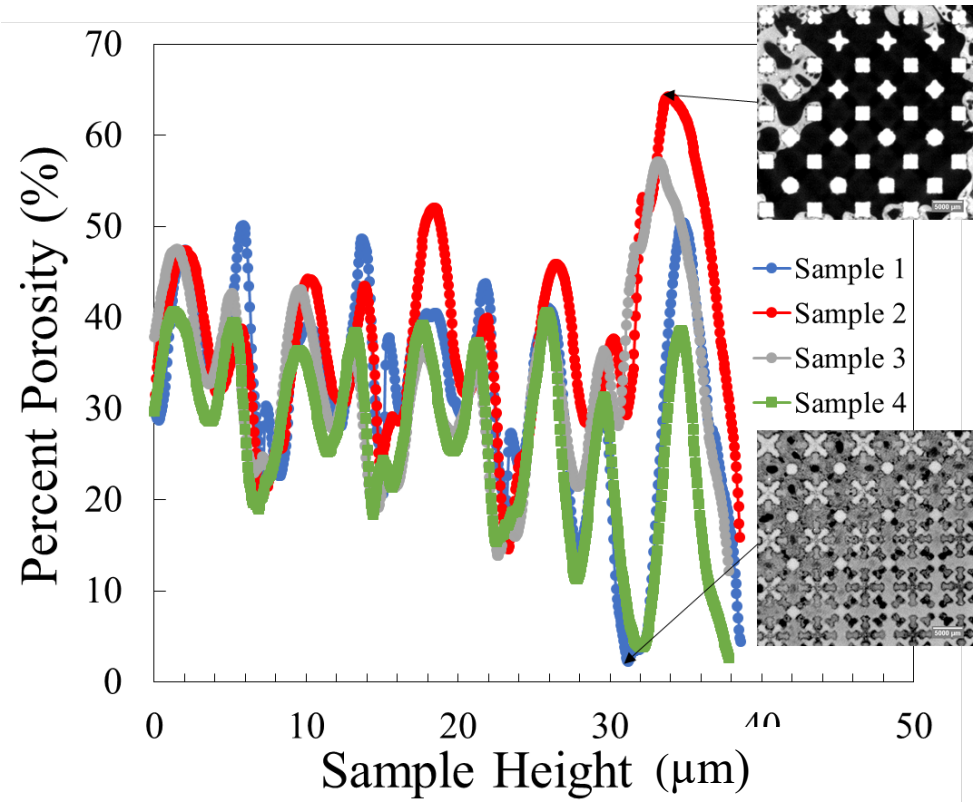

Fig. 10 Percent porosity of the geopolymer-filled trusses as a function of sample height

3.3 Micro-CT – DCPD-Infiltrated Trusses

The quantified porosity percentages for the DCPD-filled trusses were all very low with a maximum of 3.1% in sample 1, as shown in Fig. 11. Sample 2 had the lowest average porosity throughout the volume at 0.37%, and sample 4 had the highest with a measurement of 0.86%. Cracks within the DCPD matrix were observed in samples 2–4 but not within sample 1. These cracks were likely formed due to the thermal stresses upon cooling as the DCPD cured.

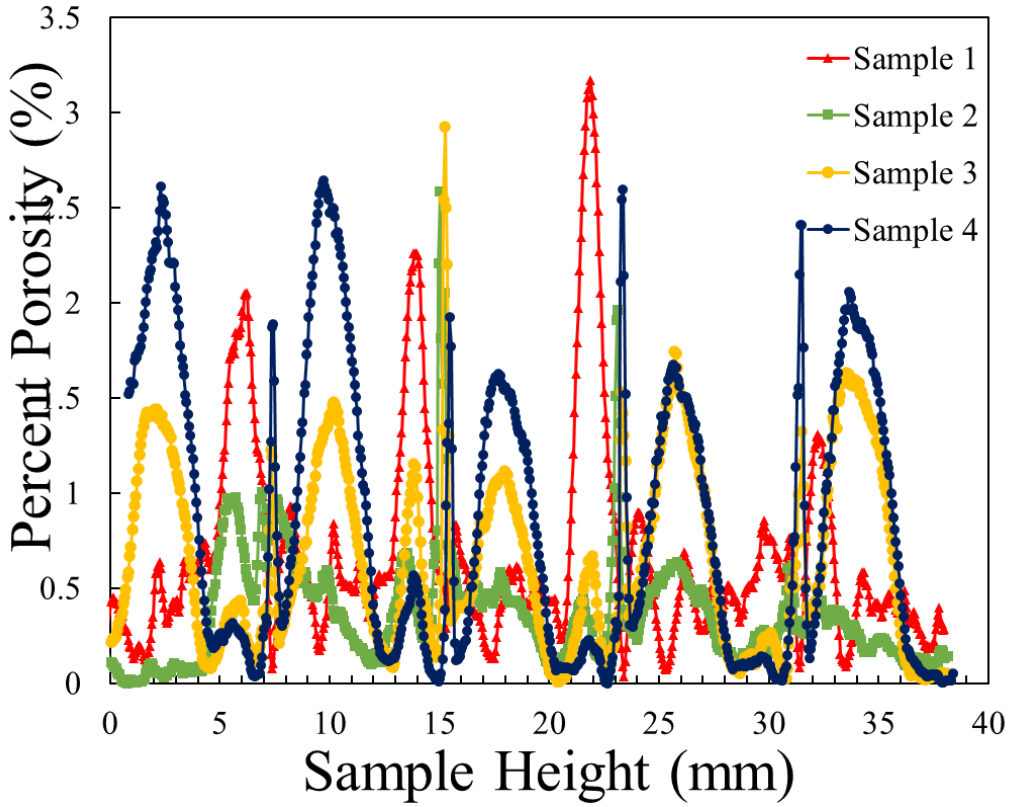

Fig. 11 Percent porosity as a function of height for the DCPD-filled trusses

4. Compression Testing Results

4.1 As-Built Trusses

Compression testing was the test method of choice, as it has been shown that the most important property when designing impact-resistant structures is compressive strength.[14] Compression testing was performed using an Instron 1332 servohydraulic test machine. In addition, digital image correlation (DIC) was used to measure full-field surface strains. The as-built trusses did not show much ductility, and the failure mode was characterized by failure along a 45° shear plane and the trusses shattering into a number of pieces (Figs. 12 and 13, respectively). The results of this testing are shown graphically in Fig. 14.

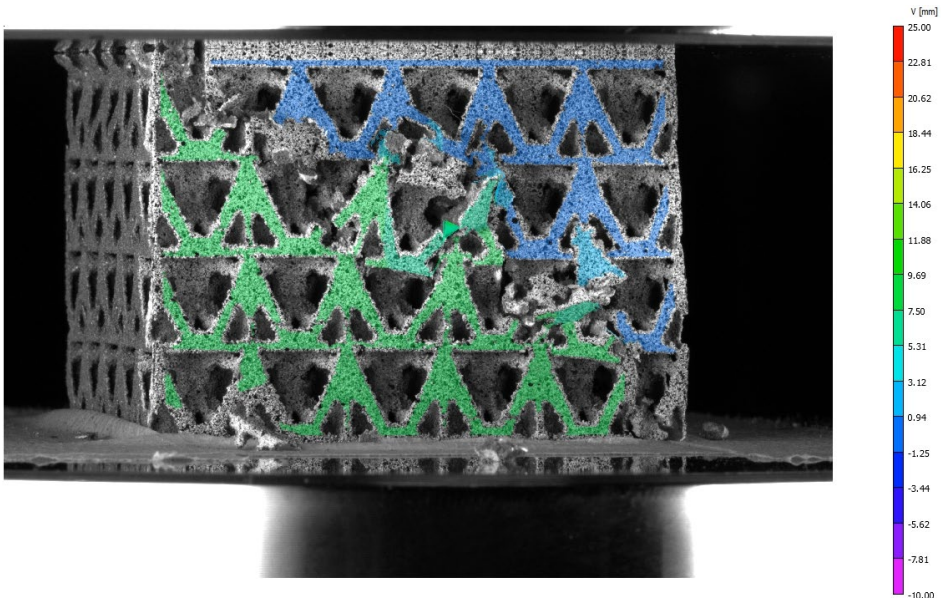

Fig. 12 Compressive failure of the uninfiltrated aluminum trusses occurred along a 45° plane

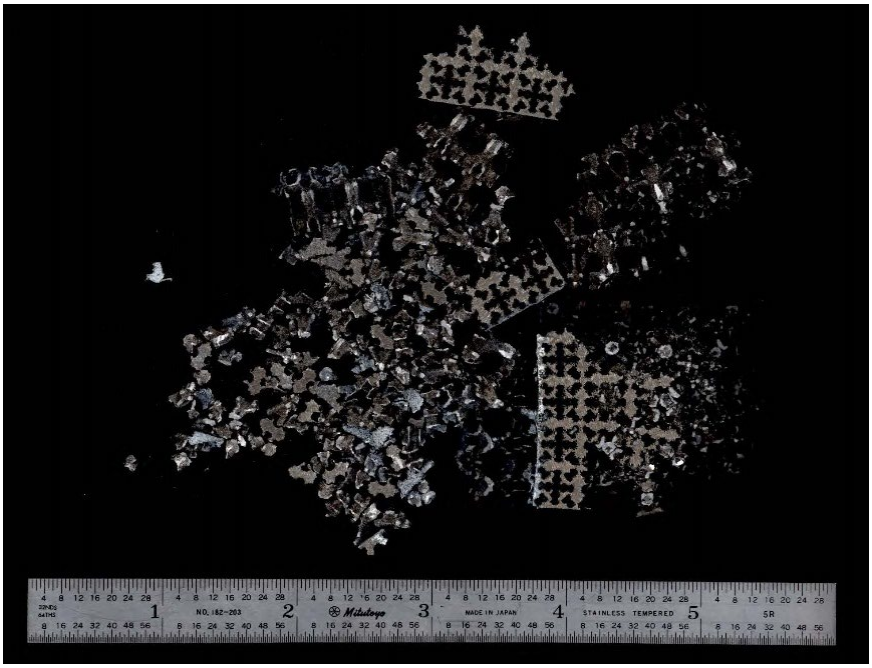

Fig. 13 Representative failure mode of compression tested as built and heat-treated aluminum trusses

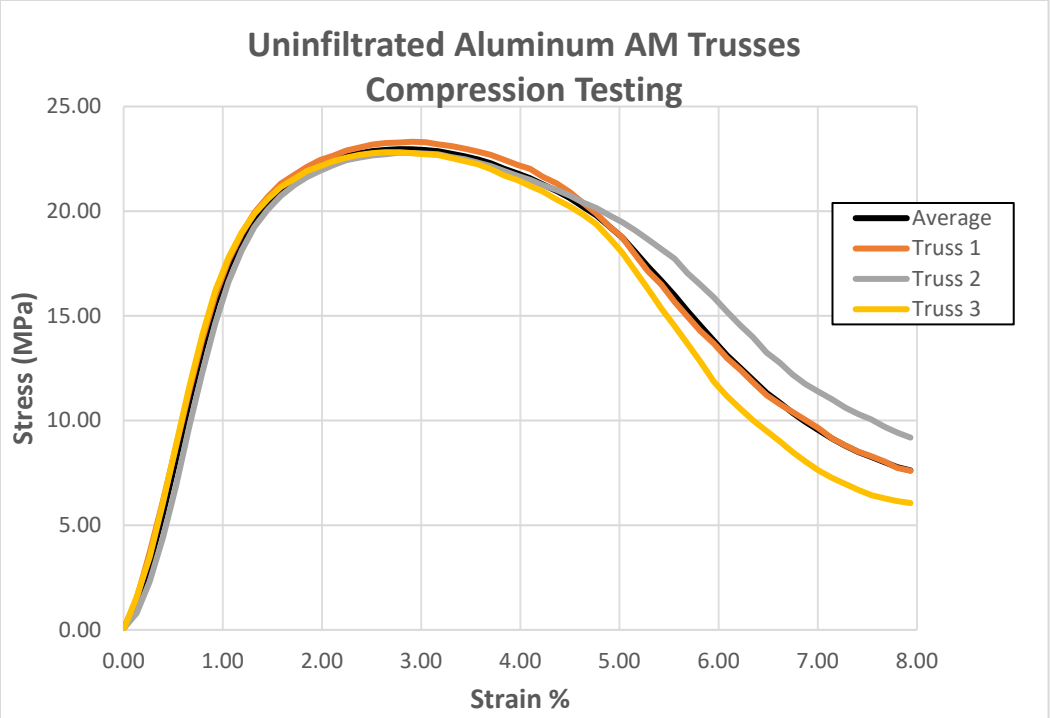

Fig. 14 Compression data generated from testing as-built 40-mm cubed aluminum trusses

4.2 LTS-Infiltrated Trusses

The same equipment and process described in Section 4.1 was used to test the LTS-infiltrated trusses. The blocks showed compressive failure on a 45° shear plane (see Fig. 15), which is consistent with Brodin and Saarimäki,[15] which states that hybrid lattice structures tend to fail due to a shear mechanism between the struts along preferred planes. Figure 16 shows the principal strains as obtained from DIC measurements for sample 2. The full-field strain measurements clearly indicate where the onset of truss collapse and correlates well to the approximate locations where the highest percent porosity, as presented in Fig. 9. In addition, as depicted from the DIC strains, higher strain values follow along the contour of the trusses, which indicates that the trusses carry a significant amount of the loads. The results of this testing are shown graphically in Fig. 17. The axial strains shown in the graph are determined from the machine actuator stroke. These results were compared to the results of compression testing 40-mm cubes of just the LTS. As shown in Fig. 18,[16] the infiltrated trusses achieved higher strength levels, and more ductility than LTS alone.

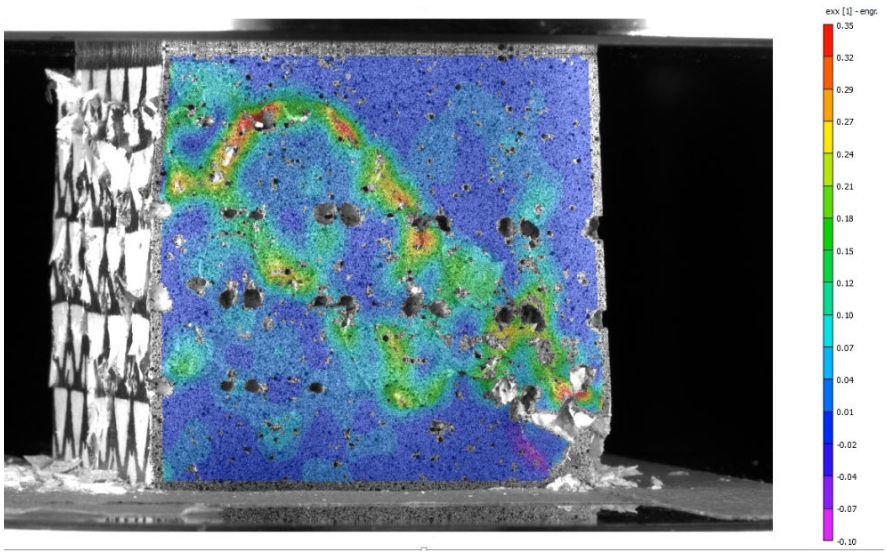

Fig. 15 Compressive failure of the LTS-infiltrated aluminum trusses occurred along a 45° plane

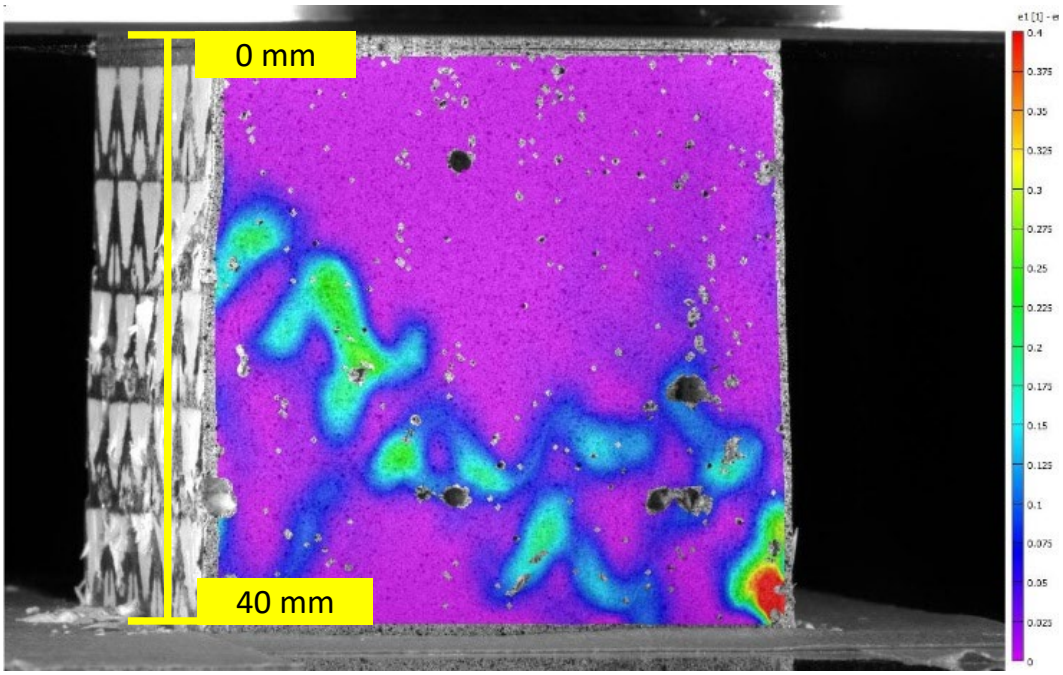

Fig. 16 Full-field principal strains for sample 2. The strains correlate to the approximate location of the higher percent porosity as depicted in Fig. 9.

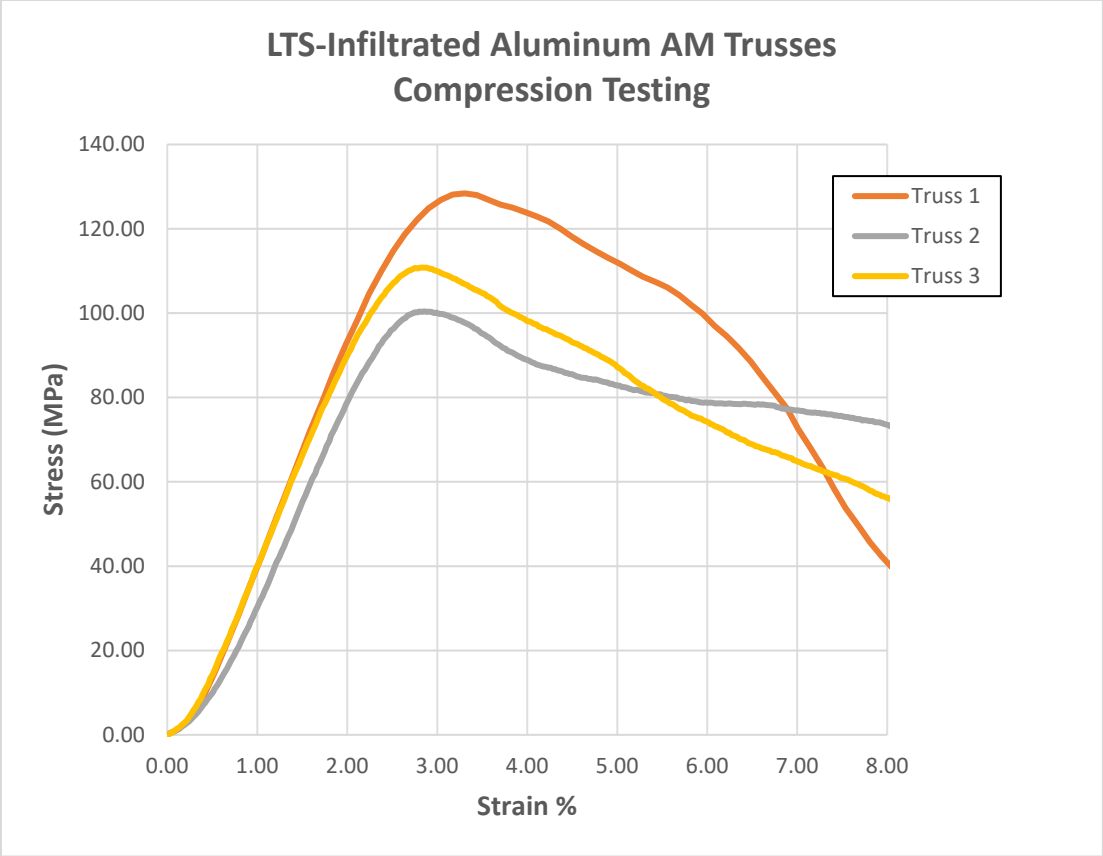

Fig. 17 Compression data generated from testing LTS-infiltrated 40-mm cubed aluminum trusses

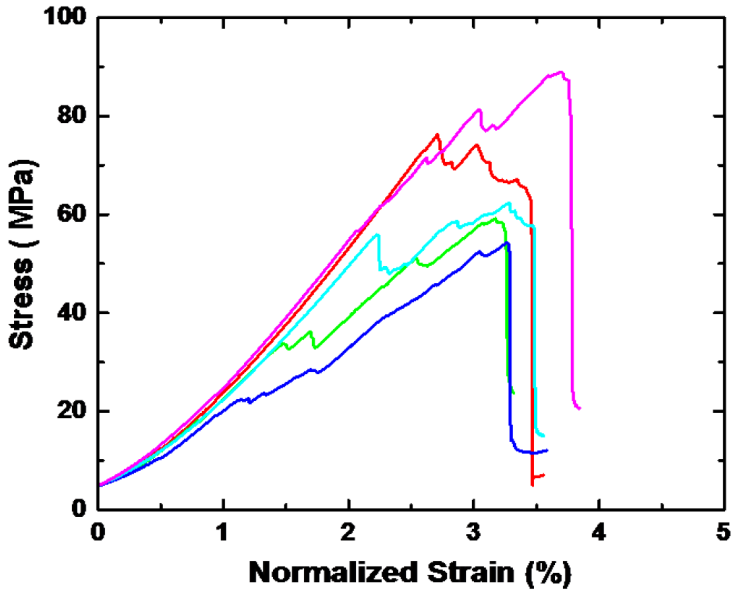

Fig. 18 Compression data generated from testing 40-mm cubes of LTS alone[16]

As shown, the compressive strength and ductility of the LTS-infiltrated aluminum trusses is higher than that of the LTS material itself. In addition, because of this increased ductility, fracture does not occur instantaneously, as with the LTS alone. Even though the strength peaks at about 3.5% strain for each instance, the infiltrated truss continues to strain after this maximum point.

4.3 Geopolymer-Infiltrated Trusses

The geopolymer-infiltrated trusses showed crumbling during compression testing (Fig. 19) and did not achieve the stress levels attained by the LTS. The geopolymer material reacted with moisture in the air, which caused oxidation build-up at the surface. Hence, the typical DIC speckling pattern methods could not be applied to these set of experiments. As shown, these blocks also failed in compression on a 45° shear plane. The results of this testing are shown graphically in Fig. 20. Similarly, the axial strains are derived from the actuator displacements.

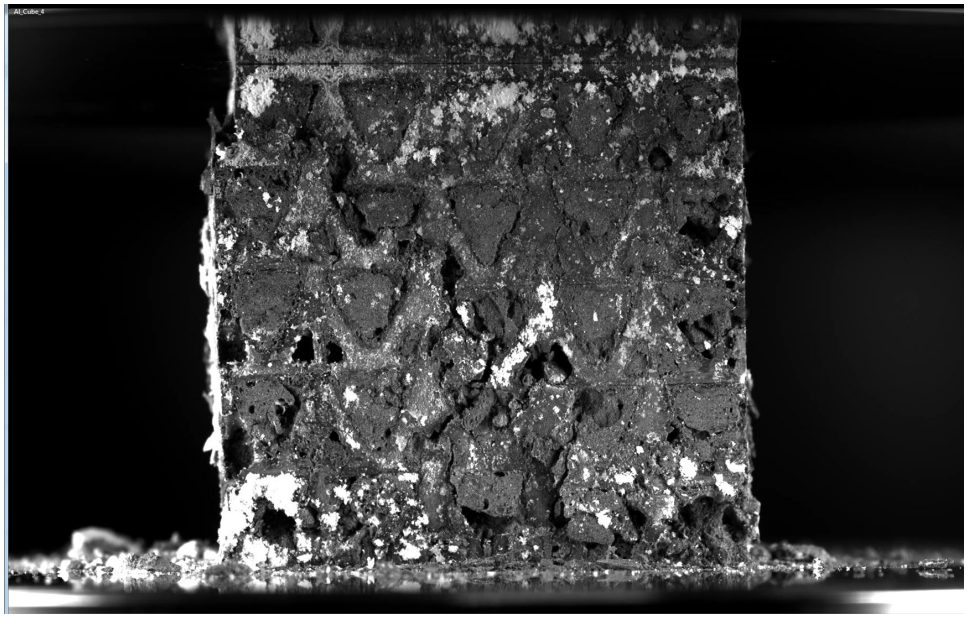

Fig. 19 Compressive failure of the geopolymer-infiltrated aluminum trusses occurred along a 45° plane. Much crumbling of the geopolymer was noted.

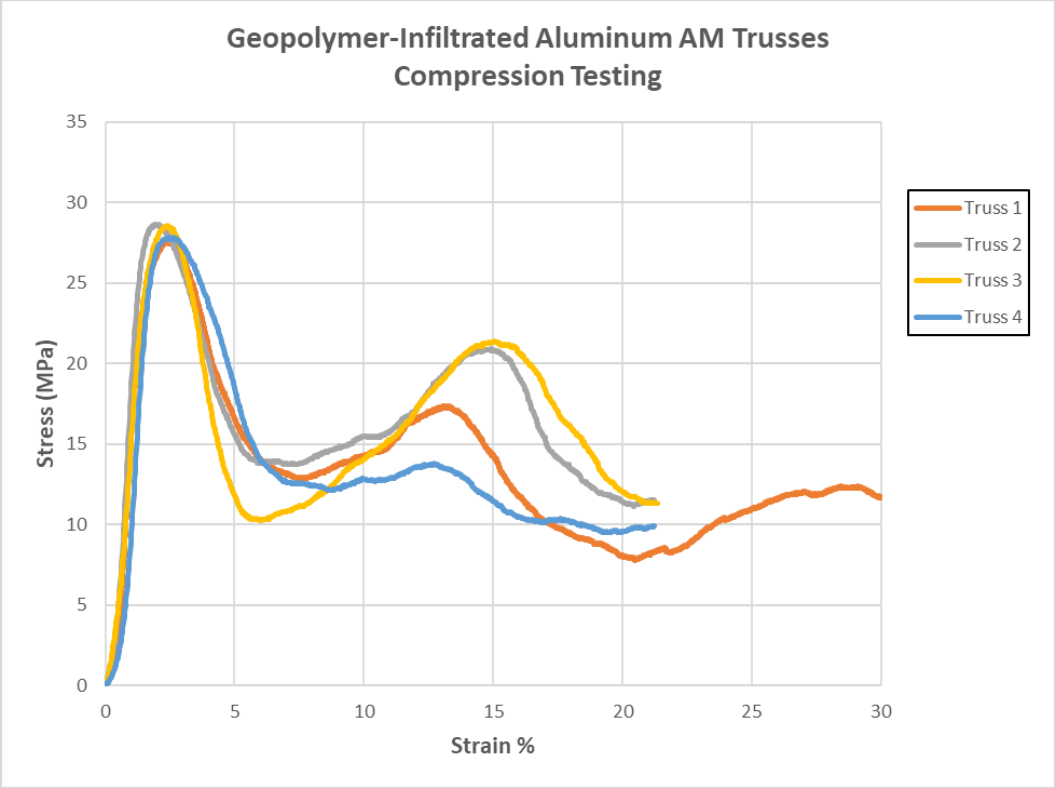

Fig. 20 Compression data generated from testing geopolymer-infiltrated 40-mm cubed aluminum trusses

4.4 DCPD-Infiltrated trusses

For the DCPD-infiltrated trusses, it was not as apparent that failure occurred on a 45° shear plane, as the samples tended to show increased ductility over the LTS- and geopolymer-infiltrated trusses and showed "barreling" as a failure mode instead (Fig. 21). Here, the DIC results reveal a much more uniformly distributed loading condition. The strains (in green) directly over the DCPD are about even across the entire face. This is also true for the strains (blue) on the truss members. The results of this testing are shown graphically in Fig. 22. The DCPD provided the added benefit of containing the failed truss ligaments during testing. More so, the trusses act as reinforcements for the DCPD polymer. The yield behavior for the DCPD-infiltrated trusses averages 86.8 ± 5.76 MPa, which is about 18% higher than yield strengths reported by Knorr et al. for neat DCPD.[17] Even at strains up to about 40%, the samples remained completely intact.

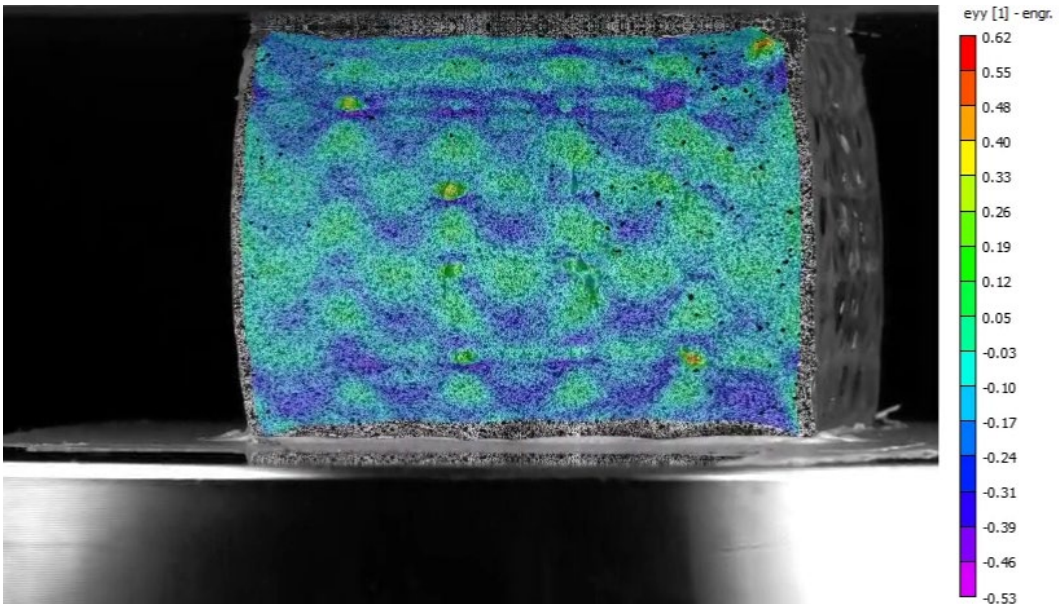

Fig. 21 Compressive failure of the DCPD-infiltrated aluminum trusses showed barreling

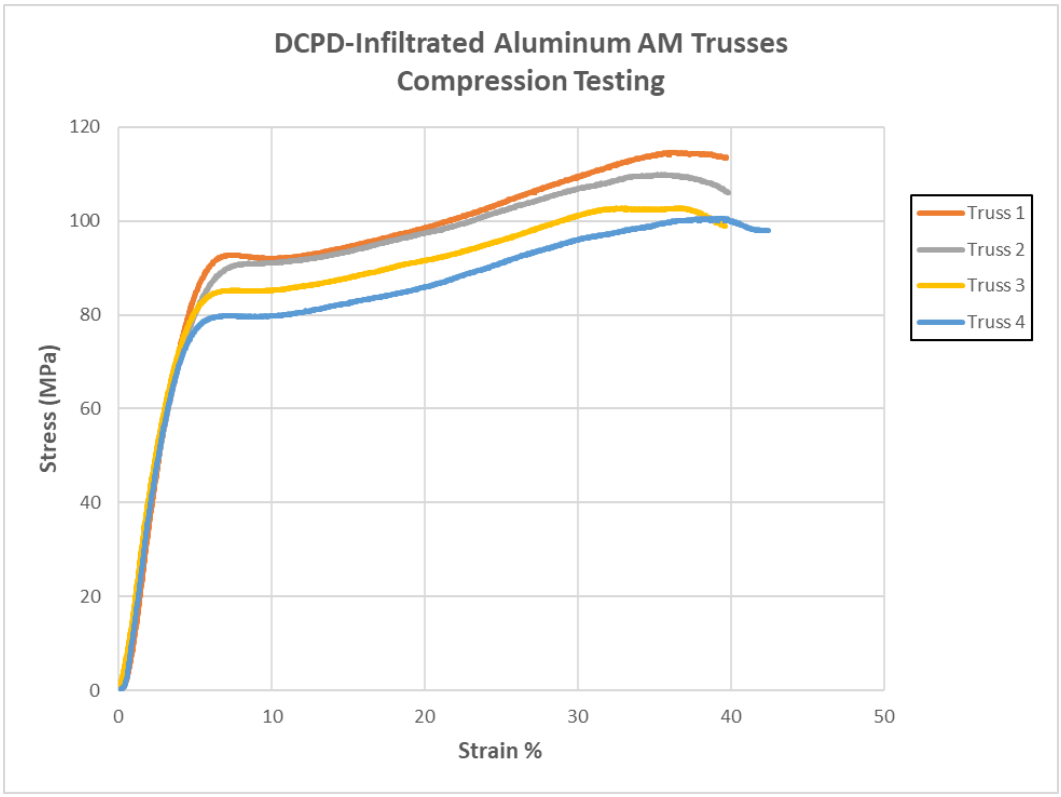

Fig. 22 Compression data generated from testing DCPD-infiltrated 40-mm cubed aluminum trusses

All of the compression test results were plotted as shown on Fig. 23 for comparative purposes. As shown, the geopolymer infiltration did not provide improved compressive test results over the uninfiltrated metallic truss. The LTS-infiltrated truss showed much-improved stress levels (compared to geopolymer-infiltrated and uninfiltrated trusses) but did not exhibit much strain. The DCPD-infiltrated trusses provided the best combination of compressive stress and strain.

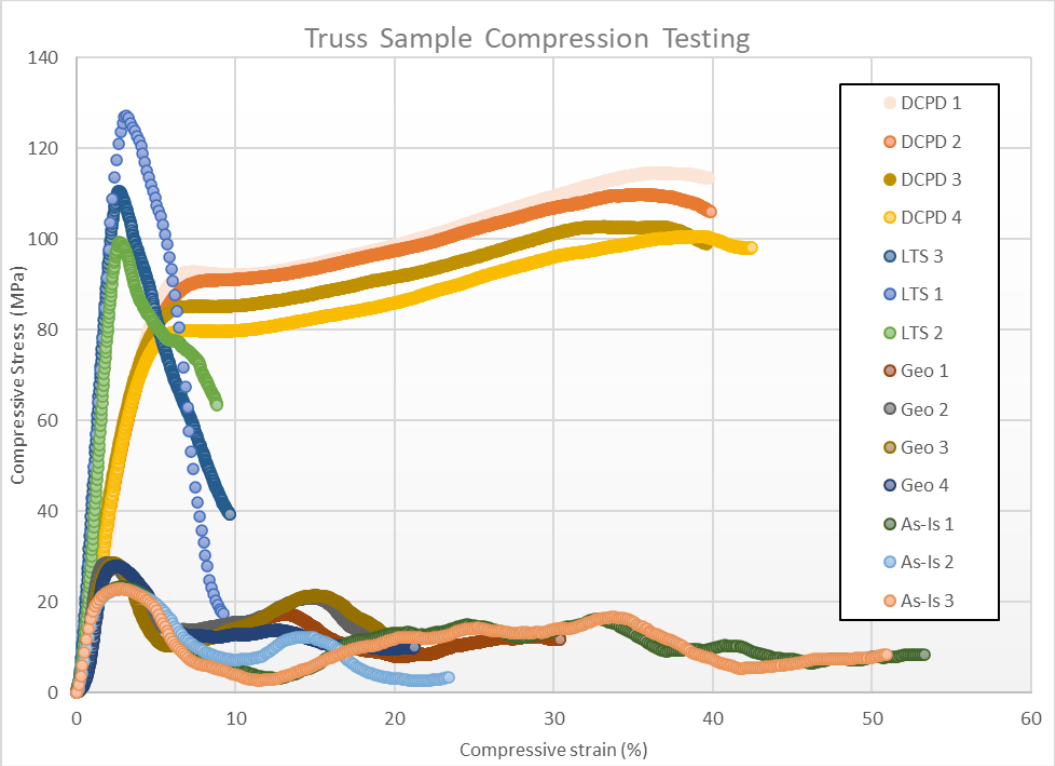

Fig. 23 Compression data generated from all 40-mm cubed aluminum trusses

5. Discussion

Testing of the as-built and infiltrated trusses demonstrated potential areas of improvement for the truss design. First, as porosity was closely correlated with compression strength, the truss design should be altered to enable better infiltration. Design of the unit cell to avoid or minimize overhangs <45° (i.e., "self-supporting geometry") and minimum wall thickness (avoiding struts <0.5 mm thick and x aspect ratio (for this material) will produce a more robust part. Examples of this can be seen in the vertical strut that did not survive the recoating forces during the build. Topology optimizations that incorporate AM constraints for self-supporting angles are available today in commercial software. Interface porosity could be reduced through optimized contour and down-skin parameters for improved surface finish or via postprocessing steps to remove partially melted particles and remove

additional surface material for a smoother finish. Another approach is to simply reduce the target volume fraction of the design during the topology optimization process. Reducing the volume fraction increases the volume of void, thus facilitating infiltration. A second, though more difficult approach may be to incorporate a model of the infiltration process into the optimization and perform a multi-objective optimization whereby both compressive strength and porosity are optimized. Further, the design optimization may be adapted to AM processes to hopefully avoid porosity in the truss and residual stress.[18] Finally, the material model used for the optimization was linear elastic, and a more sophisticated model with a nonlinear material response and failure (if it exists in commercially available software) may be incorporated to improve the design under extreme compressive loading. In addition, there are newer aluminum alloys for DMLS with better ductility. AlSi10Mg is intended for lightweight parts needing good thermal properties.

The overall porosity percentages calculated from the micro-CT data for the LTS-filled trusses did not correlate with the peak compression strength, but the maximum porosity within an individual 2-D layer through the height did match with the failure order. As seen in Fig. 9 and discussed in Section 3.1, sample 2 had the highest peak porosity throughout the sample height, followed by samples 3 and then 1. The sample with the highest peak porosity had the lowest compression strength, indicating that the peak porosity within a given layer through the height may lead to the onset of failure and may be a viable method to predict the sample strength.

There were no observed correlations between the geopolymer-filled porosity calculations from micro-CT and the compression test results. This is likely due to the large variability for the degree of infiltration and the very similar peak compression stresses that are close to the compression strengths of the unfilled trusses.

The DCPD filled trusses had both porosity of unfilled regions as well as cracking of the DCPD resin observed in samples 2–4. Sample 1 did not have any observed cracking and had the highest compression strength. Porosity quantifications from samples 2–4 correlated with the compression strength data with the highest average percent porosity (0.86% for sample 4) relating to the lowest strength. It was also observed that the maximum peaks within the porosity profile throughout the sample height alternated between peaks due to unfilled regions and peaks due to DCPD cracking. This is illustrated in Fig. 24, demonstrating the microstructural changes as a function of sample height of the DCPD-filled sample 4. The broader peaks are related to the cracking within the resin and the sharp, narrow peaks are unfilled regions. Comparing the DCPD micro-CT results of Fig. 11 with the compression

testing results of Fig. 22, it appears that the magnitude of resin cracking is the dominant mechanism for failure and for compression strength predictions.

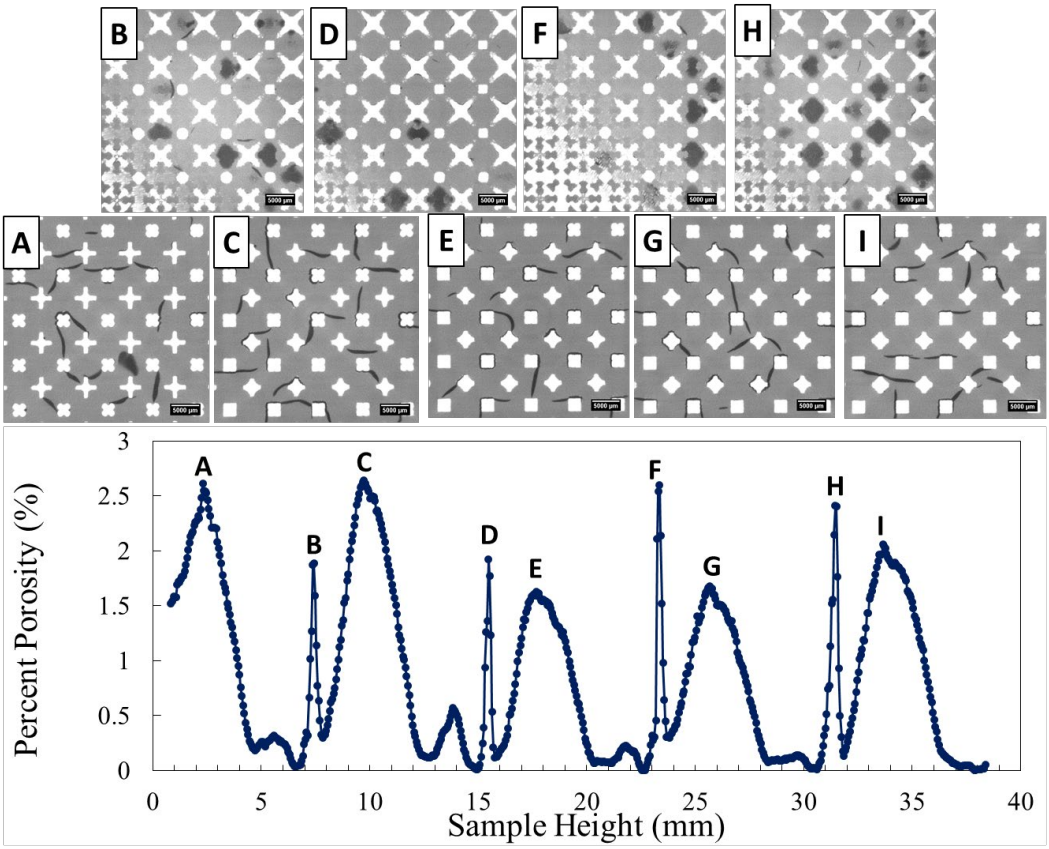

Fig. 24 DCDP-filled truss sample 4, illustrating that the broader peak percentages are due to resin cracking, and the sharper, narrower peaks are due to unfilled pores

6. Conclusions

- Micro-CT inspection allowed for a qualitative comparison of the infiltrated trusses and a means of predicting which trusses (within groups of LTS of DCPD-filled trusses) would exhibit higher compressive strength. The compression strengths of the LTS-filled trusses corresponded with the peak porosity within a given layer through the sample height and the DCPD truss strength matched well with the extent of resin cracking.
- Compression testing showed that AM aluminum trusses infiltrated with DCPD provided the best combination of stress and strain compared to un-infiltrated trusses and those infiltrated with a LTS ceramic and a geopolymer. The LTS offered the best yield strength response.

7. Future Work

To expand on these results, ballistic and/or blast testing could be performed on DCPD-infiltrated trusses to determine the feasibility of this type of protection on the battlefield. Additionally, controlled resin-curing experiments could be performed to minimize the cracking within the sample and further enhance the strength.

8. References

1. US Army Public Affairs. Secretary of the Army approves new advanced manufacturing policy; 2019 Oct 4. https://www.army.mil/article/228151 /secretary_of_the_army_approves_new_advanced_manufacturing_policy.

2. Marar K, Eren O, Celik T. Relationship between impact energy and compression toughness energy of high-strength fiber-reinforced concrete. Mater Lett. 2001 Feb;47:297–304.

3. Hadi A, Vignat F, Villeneuve F. Design configurations and creation of lattice structures for metallic additive manufacturing. 14éme Colloque National AIP PRIMECA; 2015 Mar.

4. Rosen D, Johnston S, Reed M, Wang H. Design of general lattice structures for lightweight and compliance applications. Proceedings of the Rapid Manufacturing Conference; 2006.

5. Liu K, Tovar A. An efficient 3D topology optimization code written in Matlab. Struct Multidisciplinary Optim. 2014;50(6):1175–1196.

6. Wildman RA. Postprocessing of voxel-based geometry algorithms library (CGAL). Army Research Laboratory (US); 2015. Report No.: ARL-MR-0892.

7. Manfredi D, Calignano F, Krishnan M, Canali R, Ambrosio EP, Biamino S, Ugues D, Pavese M, Fino P. Additive manufacturing of Al alloys and aluminum matrix composites (AMCs). In: Monteiro WA, editor. Light metal alloys applications. InTech; 2014. Chapter 1.

8. Martukanitz R. Penn State University. Personal communication, 2016 Sep 30.

9. Bates T. Rutgers' Richard Riman co-invented energy-efficient technology that could help limit climate change. 2017 Feb 13. https://www.rutgers.edunews /rutgers-develops-eco-friendly-concrete.

10. He J, Zhang J, Yu Y, Zhang G. The strength and microstructure of two geopolymers derived from metakaolin and red mud-fly ash admixture: a comparative study. J Constr Build Mater. 2012;30:80–91.

11. Woodson CS, Grubbs RH, inventors; Cymetech LLC, assignee. Polymerization of low grade DCPD monomers using an olefin metathesis catalyst. United States patent US 6020443A. 2000 Feb.

12. Toplosky VJ, Walsh RP. Thermal and mechanical properties of poly-dicyclopentadiene (DCPD) at cryogenic temperatures. American Institute of Physics AIP Conference Proceedings. 2006 Apr;824(1).

13. Sands J, Knorr D, DEVCOM Army Research Laboratory. Personal communication, 2022 July 12.

14. Lane R, Craig B, Babcock W. Material ease: materials for blast and penetration resistance. AMPTIAC Quarterly. 2003;6(4).

15. Brodin H, Saarimäki J. Mechanical properties of lattice truss structures made of a selective laser melted superalloy. Presented at the 13th International Conference of Fracture; 2013 June.

16. Pepi M, Riman R, Whalen T, Brennan R, Bratcher M. Enabling in-theater processes for indigenous, recycled, and reclaimed material manufacturing. Army Research Laboratory (US); 2015 Dec. Report No.: ARL-TR-7560.

17. Knorr DB Jr, Masser KA, Elder RM, Sirk TW, Hindenlang MD, Yu JH, Richardson AD, Boyd SE, Spurgeon WA, Lenhart JL. Overcoming the structural versus energy dissipation trade-off in highly crosslinked polymer networks: ultrahigh strain rate response in polydicylopentadiene. Compos Sci Tech. 2015;114:17–25.

18. Wildman RA, Gaynor AT. Topology optimization for reducing additive manufacturing processing distortions. Army Research Laboratory (US); 2017. Report No.: ARL-TR-8242.

List of Symbols, Abbreviations, and Acronyms

2-D	two-dimensional
Al	aluminum
AM	additive manufacturing
ARL	Army Research Laboratory
Ca	calcium
$CaSiO_3$	calcium silicate
CGAL	Computational Geometry Algorithms Library
CO_2	carbon dioxide
CT	computed tomography
DARPA	Defense Advanced Research Projects Agency
DCPD	dicyclopentadiene
DEVCOM	US Army Combat Capabilities Development Command
DIC	digital image correlation
DMLS	direct metal laser-sintering
EDM	electro-discharge machining
LTS	low-temperature solidified
Mg	magnesium
micro-CT	micro-computed tomography
Na	sodium
NaOH	sodium hydroxide
O	oxygen
rHLPD	reactive hydrothermal (solvothermal) liquid phase densification
Si	silicon
UCS	unconfined compressive strength

1 (PDF)	DEFENSE TECHNICAL INFORMATION CTR DTIC OCA
1 (PDF)	DEVCOM ARL FCDD RLD DCI TECH LIB
3 (PDF)	DEVCOM ARL FCDD RLW MB J SIETINS P MOY FCDD RLW MD M PEPI